ACS APPLIED MATERIALS & INTERFACES

www.acsami.org

Research Article

Freestanding Bipolar Membranes with an Electrospun Junction for High Current Density Water Splitting

Devon Powers, Abhishek N. Mondal, Zezhou Yang, Ryszard Wycisk, Eric Kreidler, and Peter N. Pintauro*

Cite This: *ACS Appl. Mater. Interfaces* 2022, 14, 36092−36104

Read Online

ACCESS | Metrics & More | Article Recommendations

ABSTRACT: Freestanding bipolar membranes (BPMs) with an extended-area water splitting junction were fabricated utilizing electrospinning. The junction layer was composed of a mixed fiber mat that was made by concurrently electrospinning sulfonated poly(ether ether ketone) (SPEEK) and quaternized poly(phenylene oxide) (QPPO), with water splitting catalyst nanoparticles intermittently deposited between the fibers. The mat was sandwiched between solution cast SPEEK and QPPO films and hot-pressed to form a dense trilayer BPM with an extended-area junction of finite thickness, composed of QPPO nanofibers embedded in a SPEEK matrix with the catalyst nanoparticles interspaced between the two polymers. The composition, ion-exchange capacity, and catalyst type/loading in the junction were varied, and the water splitting characteristics of the membranes were assessed. The best BPMs fabricated in this work employed a graphene oxide catalyst and exhibited a low trans-membrane voltage drop of about 0.82 V at 1000 mA/cm^2 in water splitting experiments with 0.5 M Na_2SO_4 and stable water splitting operation for 60 h at 800 mA/cm^2.

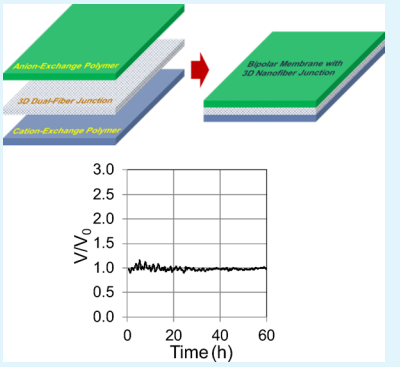

KEYWORDS: *bipolar membrane, water splitting, durability, electrodialysis, ion exchange*

1. INTRODUCTION

A bipolar membrane (BPM) is typically fabricated as a laminate of a cation-exchange polymer (CEP) layer and an anion-exchange polymer (AEP) layer with the interfacial junction containing a catalyst (e.g., polymer, metal salt, or graphene oxide particles)[1−8] that reduces the water splitting overpotential. The ability of BPMs to split water at low voltage (ideally at ∼0.83 V when the membrane separates a 1 M alkaline solution in the anodic compartment and a 1 M acid solution in the cathodic compartment) makes them attractive for a wide range of applications, such as electrodialysis salt separations and acid/base generation.

Under reverse polarization, with the anion-exchange side of the BPM contacting the anodic compartment of an electrolytic cell and the cation-exchange side in contact with the cathodic compartment, water is split into H^+ and OH^- at the bipolar junction. Hydroxide ions migrate under the influence of the electric field to the anode, whereas protons migrate to the cathode. A conventional BPM with a catalyzed 2D junction (shown schematically in Figure 1a) typically performs well at low current densities, up to ∼100 mA/cm^2, with an acceptably low transmembrane voltage drop and minimal co-ion crossover for moderately concentrated electrolyte solutions.

A number of reviews and research papers have been published which address BPM fabrication and characterization for applications in electrodialysis separations, electrolysis cells, and fuel cells.[9−12] Several studies[13−17] reported different methods of catalyzing and structuring the bipolar junction to increase the stability, selectivity, and operational current density and to minimize the transmembrane voltage drop. Arges et al.[13] employed soft lithography to create/control the interfacial area in the bipolar junction and showed that a 250 mV reduction in the water splitting onset potential could be achieved by a 2.28-fold increase in interfacial junction area. Oener et al.[14] described BPMs with junctions containing two different catalyst layers, one near the acidic polymer and the second near the alkaline polymer. This approach was different from the typical use of a single catalyst at the interface between the cation-exchange and anion-exchange polymers. The authors were able to split water at 20 mA/cm^2 with an overpotential of <10 mV and carried out pure water electrolysis experiments with an alkaline anode and acidic cathode at 500 mA/cm^2 and ∼2.2 V. In another study, Xu et al.[15] fabricated BPMs catalyzed with in situ generated, shielded Goethite $Fe^{3+}O(OH)$ nanoparticles (10−50 nm). The catalyst

Received: April 30, 2022
Accepted: July 25, 2022
Published: July 29, 2022

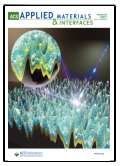

https://doi.org/10.1021/acsami.2c07680
ACS Appl. Mater. Interfaces 2022, 14, 36092−36104

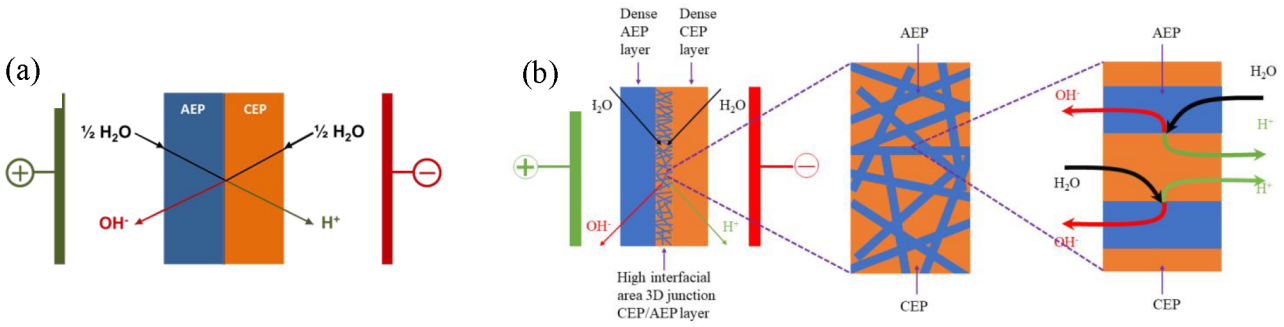

Figure 1. (a) A BPM operating in water splitting mode. (b) A 3D junction BPM.

lowered the water splitting activation energy from 5.15 to 1.06 eV per HO-H bond. The resulting membranes showed a low potential drop of 1.1 V at 100 mA/cm^2 and satisfactory (140 h) durability for water splitting at this current density. Tanioka et al.[16] fabricated BPMs containing an electrospun anion-exchange or cation-exchange porous fabric sandwiched between CEP and AEP films. Facile water splitting was observed with a high specific area junction layer containing both tertiary pyridyl groups and quaternary pyridinium groups, while slower water splitting was observed with a low surface area fabric containing sulfonic acid groups. Thiele et al.[17] described an interesting application of BPMs in a zero-gap water electrolyzer, where the effects of AEP layer thickness and the presence of catalyst (IrO_2) on performance were studied. When the AEP layer was reduced from 9 to 3 μm, the current density at a cell voltage of 2.2 V increased from 40 mA/cm^2 to 1600 mA/cm^2. When the bipolar junction was moved to the immediate vicinity of the anode catalyst layer, the cell current density dramatically increased to 6000 mA/cm^2 at 2.2 V. It should be noted that most/all commercial BPMs when operating as a freestanding film irreversibly degrade during high current density water splitting due to delamination (blistering/ballooning) at the AEP/CEP junction. One way to minimize or eliminate delamination at high current density is to confine a 2D junction BPM under compression between two electrodes in a membrane-electrode assembly.[14,17] Such a configuration, however, is not amenable to a conventional electrodialysis stack, and other applications where freestanding films are required.

Recently, Pintauro and co-workers introduced a novel BPM morphology with an extended 3D bipolar junction that allows for high current density water splitting operation of free-standing films.[18] The membrane was fabricated by electrospinning a trilayer film: The first layer was a nanofiber mat of sulfonated poly(ether ether ketone) (SPEEK) followed by the concurrent electrospinning of quaternized polyphenylene oxide (QPPO) anion-exchange polymer fibers and SPEEK fibers, and finally electrospinning a layer of only QPPO fibers. During dual fiber electrospinning, aluminum hydroxide catalyst nanoparticles were intermittently spray deposited between the fibers. The trilayer mat was exposed to dimethylformamide vapor and then hot pressed to close all interfiber voids, thus creating a BPM with a 3D junction layer of finite thickness composed of interlocking and interpenetrating SPPEK and QPPO fibers with dispersed catalyst particles, where the interfacial anion-exchange/cation-exchange area in the junction far exceeds the geometric membrane area footprint (see Figure 1b). In such a membrane, the water splitting current is distributed over a very high interfacial area to minimize/eliminate membrane damage (e.g., delamination) over time. Preliminary experiments showed that a 3D junction BPM could efficiently split water at current densities up to 1000 mA/cm^2 with a transmembrane voltage drop of ~1.0 V.

The present study reports on new results with freestanding 3D junction BPMs, where a new and simpler membrane fabrication method is employed using SPEEK and QPPO as the CEP and AEP materials, respectively. Rather than sequentially spin all three layers of a 3D junction BPM, only the junction layer was electrospun as a QPPO/SPEEK dual fiber mat, followed by attachment of preformed solution-cast dense outer layers of QPPO and SPEEK and the closing of all interfiber void space in the dual fiber junction layer. Using this procedure, a series of BPMs were fabricated and evaluated for water splitting, where the membranes differed in AEP and CEP ion-exchange capacity (IEC), the relative amounts of AEP and CEP in the junction layer, and the type and loading of catalyst in the junction. Current−voltage polarization data and a constant current long-term water splitting experiment were used to assess the BPMs. In general, BPMs made using the new fabrication method worked well, with (i) water splitting at high current densities (up to 1 A/cm^2) with a low transmembrane voltage drop (generally <1.0 V), (ii) minimal co-ion crossover (≤1.0 mA/cm^2), and (iii) stable long-term operation with no delamination/degradation during a constant current water splitting experiment.

2. EXPERIMENTAL SECTION

2.1. Materials. All materials to prepare QPPO and SPEEK were purchased from commercial vendors. Poly(ether ether ketone) (PEEK) was obtained from Evonik, and poly(2,6-dimethyl-1,4-phenylene oxide) (PPO) was obtained as a dry powder from Sigma-Aldrich. Reagent-grade concentrated sulfuric acid, chlorobenzene, bromine, dimethylacetamide, dimethylformamide, dimethyl sulfoxide, methanol, poly(4-vinylpyrrolidone) (PVP, MW = 1,300,000 g/mol), 4.2 M trimethylamine (TMA) in ethanol, and 6.0 M TMA in water were used as received from Sigma-Aldrich. Nanographene oxide powder was purchased from the Graphene Supermarket (Ronkonkoma, NY), where the platelets had a lateral size in the 90−200 nm range and a thickness of ~1 nm. $Al(OH)_3$ (10 nm), Al_2O_3 (20 nm), and $Zr(OH)_4$ (40 nm) nanoparticles were purchased from US Research Nanomaterials Inc. (Huston, TX).

2.2. Preparation of Ionomers. SPEEK was prepared by sulfonating PEEK in concentrated sulfuric acid, as described in the literature.[19,20] Dry PEEK and concentrated sulfuric acid were combined in a glass jar with a Teflon-lined cap. After initial agitation, the jar was rolled for up to 216 h (9 days) at room temperature. During this time, the solution became transparent and then reddish-brown in color. The sulfonation was terminated by slowly pouring the solution into 0 °C deionized water. The solid product precipitate was

https://doi.org/10.1021/acsami.2c07680
ACS Appl. Mater. Interfaces 2022, 14, 36092−36104

washed with DI water numerous times to remove trace amounts of acid and then dried at ambient conditions.

QPPO was synthesized by bromination and subsequent amination of PPO, as described by Xu and co-workers.[21] Fifteen g of dry PPO was dissolved in 100 mL of chlorobenzene. The solution was heated to 165 °C under reflux, and upon boiling, a Br_2/chlorobenzene solution (8.5 g Br_2 mixed with 10 mL chlorobenzene) was added dropwise to the reaction vessel. The bromination reaction was allowed to proceed for 4.5 h in an argon atmosphere. After completion of the reaction, solid Br-PPO was collected by precipitating the polymer in methanol. The degree of bromination was determined by ^{1}H NMR. Amination was performed by allowing 5 g of Br-PPO to soak for 7 days in a mixture of 100 mL of aqueous TMA and 100 mL of TMA in ethanol with occasional agitation.

2.3. Characterization of Cation and Anion-Exchange Polymers. In initial experiments, the ionic conductivity, gravimetric water uptake, and IEC of solution-cast SPEEK and QPPO films were determined. SPEEK films were preconditioned by soaking for 12 h in a room temperature 1.0 M H_2SO_4 solution (to ensure that all sulfonate ion-exchange sites were in the H^+ form), followed by thorough soaking in multiple aliquots of DI water. QPPO films were soaked for 12 h in 0.1 M NaOH and then washed numerous times with DI water, followed by immersion in a closed container containing water that had been degassed for 3 h to remove dissolved CO_2.

Ionic conductivity (H^+ for SPEEK and OH^- for QPPO) of water-equilibrated films was determined by an AC impedance method. In-plane conductivity was measured after loading a membrane sample into a BekkTech 4-electrode test cell and then submerging the cell in DI water at room temperature (QPPO was immersed in degassed water). A Nyquist plot was generated from which the membrane impedance was extracted. Ionic conductivity was determined using eq 1:

$$\sigma = L/wtR \tag{1}$$

where σ (S/cm) is the ionic conductivity, L (cm) is the distance between the electrodes, w (cm) and t (cm) are the width and thickness of the membrane sample, and R (Ω) is the measured membrane resistance (impedance) taken as the real axis value at the high-frequency intercept on the Nyquist plot.

Gravimetric water uptake was determined by measuring the mass of a membrane sample before and after equilibration in room temperature water. Uptake was determined using the following equation, where m_{wet} and m_{dry} correspond to the wet and vacuum-dried mass of the membrane, respectively:

$$\text{uptake}\,(\%) = \frac{m_{wet} - m_{dry}}{m_{dry}} \times 100 \tag{2}$$

The gravimetric concentration of fixed charge sites (IEC) of SPEEK was determined using an acid/base titration method. A proton-form SPEEK membrane sample of known dry mass was submerged in 2.0 M NaCl for 48 h, during which time protons in the membrane were exchanged for Na^+ ions. The soak solution was then titrated for H^+ using a standardized 0.01 N NaOH. The membrane IEC (mmol/g) was determined using the following equation, where V (L) is the volume of titrant required to neutralize the soak solution, N (mmol/L) is the normality of the titrant, and m_{dry} (g) is the dry mass of the membrane sample:

$$\text{IEC} = \frac{VN}{m_{dry}} \tag{3}$$

The IEC for QPPO was determined via the Mohr titration method, as described in the literature.[22] A dense QPPO film in the Cl^- form was repeatedly equilibrated multiple times in 0.2 M $NaNO_3$ to ensure that the entire sample was in the NO_3^- counterion form. All of the soak solutions were combined and titrated for Cl^- using 0.01 N $AgNO_3$ with K_2CrO_4 as the end point indicator. IEC was calculated using eq 3, where V (mL) is the volume of $AgNO_3$ titrant, N (mmol/L) is the normality of the $AgNO_3$ solution, and m_{dry} (g) is the dry mass of the QPPO film.

The volumetric concentration of fixed charges in SPEEK and QPPO (χ, with units of mmol/cm^3 of water in the polymer) was found by combining the IEC with gravimetric swelling data (g of water per g of dry membrane) and the density of bulk water (ρ_{H_2O}):

$$\chi = \frac{\text{IEC}}{\text{swelling}/\rho_{H_2O}} \tag{4}$$

2.4. Preparation of the Electrospun Bipolar Junction Layer. Bipolar junctions were prepared by concurrently electrospinning SPEEK and QPPO solutions onto a common collector while periodically spraying catalyst particles (either $Al(OH)_3$, $Zr(OH)_4$, Al_2O_3, or nanographene oxide). The electrospinning apparatus is shown schematically in Figure 2 and consisted of a rotating and

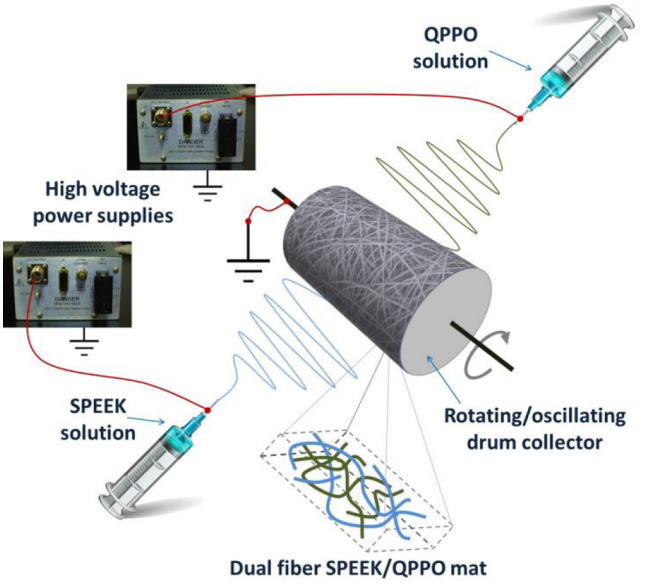

Figure 2. Schematic of the dual fiber electrospinning setup employed for the 3D bipolar junction mat fabrication.

laterally oscillating drum collector, two high voltage power supplies, and two syringe pumps. The SPEEK electrospinning solution was prepared by dissolving the polymer in DMAc solvent at room temperature. The addition of a carrier polymer has been shown to aid in the formation of electrospun proton-exchange polymer fibers.[23] In the present study, a small amount of poly(vinylpyrrolidone) (PVP) carrier was added to the SPEEK/DMAc mixture such that the final electrospinning solution had a 96:4 (wt:wt) ratio of SPEEK:PVP with an overall solids content of 17.5 wt %. Similarly, PVP was added to a QPPO/DMAc electrospinning solution, where the final QPPO:PVP (wt:wt) ratio was 98:2 and the overall solids content was 25 wt %. Catalyst particles were periodically airbrush sprayed onto the SPEEK/QPPO fiber mat during dual fiber electrospinning using a 10 wt % particle dispersion in water. The CEP/AEP composition of the junction layer was controlled by adjusting the relative flow rates of the SPEEK/QPPO solutions during electrospinning. The electrospinning parameters for one junction layer (one SPEEK/QPPO composition) are shown in Table 1.

2.5. Preparation of Dense SPEEK and QPPO Films. Dense SPEEK and QPPO films, to be used as the outer layers of BPMs, were fabricated by solution casting on a glass plate with a wet film applicator from BYK Instruments (USA). The SPEEK solution concentration was 8 wt % in DMSO and the QPPO solution concentration was 10 wt % in DMSO:MeOH (4:1 ratio by weight). The films were dried in a convection oven at 60 °C overnight, peeled off the glass plate, and used without any additional processing. The thickness of the dry films was in the 20−30 μm range.

https://doi.org/10.1021/acsami.2c07680
ACS Appl. Mater. Interfaces 2022, 14, 36092−36104

Table 1. Electrospinning Parameters for BPM Dual Fiber Junctions with SPEEK and QPPO

parameter	SPEEK	QPPO
voltage (V)	15	15
flow rate (mL/h)	0.15	0.25
spinner-to-collector distance (cm)	10.5	10.5
solution concentration (wt %)	17.5	25
solvent	DMAc	DMAc
ionomer:PVP ratio	96:4	98:2

2.6. Preparation of Bipolar Membranes. Preformed solution-cast dense films of QPPO and SPEEK were hot-pressed onto a dual fiber bipolar junction layer. Prior to hot-pressing, the junction layer was exposed to 1:1 DMAc:MeOH solvent vapor for 15 min at room temperature to soften the SPEEK fibers, and the dense QPPO film was exposed to 1:3 DMAc:MeOH solvent vapors for 15 min at room temperature. After solvent exposure, the entire three-layer assembly (QPPO film, dual fiber junction layer, and SPEEK film) was hot pressed for 15 min at 40,000 lbs and 141 °C. During hot pressing, the solvent swollen SPEEK fibers in the junction layer melted, flowed, and filled all voids between QPPO fibers and catalyst particles. The densified fiber junction and the outer/dense QPPO and SPEEK films also bonded together. The resultant dense and translucent BPM was then submerged in 0.5 M Na_2SO_4 for 1−3 h prior to a water splitting experiment. All BPMs reported in this study had a dry thickness in the 44−58 μm range.

2.7. SEM Imaging. Surface and cross-section imaging of electrospun mats and membrane samples were performed using a Merlin (Carl Zeiss) scanning electron microscope (SEM) with a Gemini II column. Prior to scanning, the samples were sputter-coated with a thin gold layer to prevent charging of the specimens and to reduce thermal damage.

2.8. Water Splitting Experiments. Current density (i) vs voltage (V) water splitting polarization experiments were carried out in a thermostated two-compartment glass H-cell equipped with Pt/Nb flat sheet working electrodes and Ag/AgCl reference electrodes mounted inside Luggin capillaries, as shown in Figure 3. A BPM (3.14 cm^2 in area) separated two compartments filled with 60 mL of 0.5 M Na_2SO_4, where the cation-exchange side of the membrane contacted the cathode compartment solution and the anion-exchange side was in contact with the anode compartment solution. The use of reference electrodes allowed for the measurement of transmembrane voltage drop without needing to correct for voltages associated with the anode and cathode reactions and the IR voltage drop in the anolyte and catholyte solutions between the working and the tips of the reference electrode Luggin probes. The $i-V$ data at room temperature (25 °C) were collected under galvanostatic conditions. For a given current, the transmembrane voltage drop was recorded after ca. 2 min (when the voltage stabilized). The measured voltage was corrected for the small IR drop in the solution between the reference electrode Luggin probe tips and the membrane surface (a distance of ∼0.01 cm on either side of the membrane), using Ohm's law in solution ($|i| = \kappa\Delta\Phi/\Delta x$, where κ is the solution conductivity, $\Delta\Phi$ is voltage correction, and Δx is the total distance between the two reference electrodes and the membrane), and a conductivity of 0.065 S/cm for 0.5 M Na_2SO_4 (calculated from equivalent ionic conductances). H-cell water splitting experiments were also used to investigate co-ion leakage, which reflects the degree of BPM permselectivity. These experiments were carried out using aqueous solutions of Na_2SO_4 (0.5 and 1.0 M) and $NaNO_3$ (1.0 and 2.0 M). The first limiting current density in an $i-V$ curve was identified (the current below the water splitting onset potential), which is a measure of cation and/or anion leakage.[24]

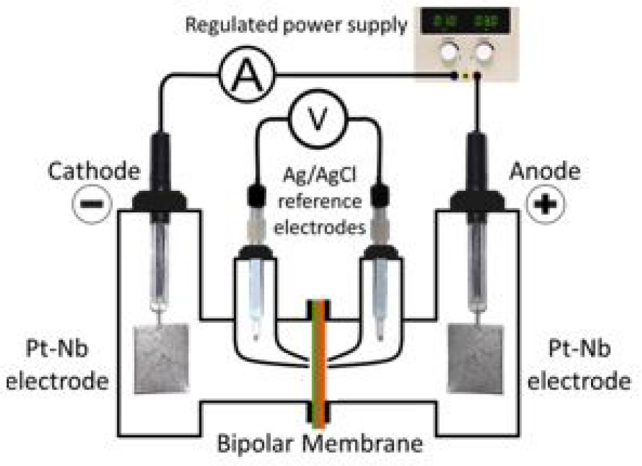

Figure 3. Schematic of the H-cell used for BPM performance and durability testing.

A BPM water-splitting durability test was performed at 30 °C and a constant current density of 800 mA/cm^2 using the two-compartment H-cell with 0.5 M Na_2SO_4 solutions in the anode and cathode chambers. The cell was operated for 8−10 h per day, with daily shutdowns overnight and daily replacements of the Na_2SO_4 electrolyte solutions. The transmembrane voltage drop was continuously monitored for 60 h of current flow operation. Current−voltage polarization data were collected before and after the durability test.

3. RESULTS AND DISCUSSION

3.1. Composition and Characterization of 3D Junction Bipolar Membranes. A total of 11 different 3D junction BPMs were fabricated and evaluated in the present study. The membranes contained 1.6 or 1.9 mmol/g IEC SPEEK and 1.4 or 1.8 mmol/g IEC QPPO. The degree of sulfonation (DS) and other key characteristics of the two SPEEK materials with the shortest and the longest sulfonation times are reported in Table 2. As expected, the longer reaction time led to a greater DS, a higher proton conductivity, and greater water uptake. The DS value for the SPEEK polymers was calculated according to eq 5, where MW_{PEEK} and MW_{SPEEK} represent the molecular weights of the PEEK (288 Da) and SPEEK (368 Da, monosulfonated) repeat unit, respectively (calculated from the chemical structures), and the IEC is that of the SPEEK polymer:[25,26]

$$DS = \frac{MW_{PEEK}IEC}{1000 + (MW_{PEEK} - MW_{SPEEK})IEC}100 \quad (5)$$

QPPO was prepared with an IEC of either 1.4 or 1.8 mmol/g, where a higher concentration of bromine during PPO bromination led to an increase in the IEC of QPPO. It was also determined that a 7-day exposure to TMA was sufficient to exhaustively aminate the brominated polymers. Characteristic properties of the two QPPO batches are listed in Table 2. An increase in IEC led to an increase in hydroxide ion conductivity and gravimetric water uptake. Although the 1.8 IEC exhibited a high water uptake of 70%, it was still a useful material for BPM fabrication because the volumetric concertation of fixed charge sites was high at 2.6 M, which would prevent significant co-ion leakage.

The composition, thickness, and type/amount of catalyst in the junction of the BPMs examined in this study are listed in Table 3. The IEC of SPEEK and QPPO fibers in the junction was always the same as that in the outer dense layers. The total dry membrane thickness was in the 44−58 μm range, with a

https://doi.org/10.1021/acsami.2c07680
ACS Appl. Mater. Interfaces 2022, 14, 36092−36104

Table 2. Properties of sulfonated PEEK and QPPO

	IEC (mmol/g)		in-plane conductivity[a] (S/cm)	gravimetric water uptake at 25 °C (%)	volumetric fixed charge concentration (χ, mmol/cm^3)
SPEEK		Degree of Sulfonation (%)			
	1.6	53	0.04	22	7.3
	1.9	65	0.07	25	7.6
QPPO		Degree of Bromination (%)			
	1.4	25	0.02	47	3.0
	1.8	36	0.04	70	2.6

[a]In water at 25 °C.

Table 3. Composition and Thickness of SPEEK/QPPO BPMs in This Study

BPM	SPEEK IEC (mmol/g)	QPPO IEC (mmol/g)	SPEEK content in the junction (wt %)	SPEEK/junction/QPPO thickness (μm)	catalyst type; areal loading; volumetric loading
A	1.6	1.4	30	20/11/20	$Al(OH)_3$; 0.5 mg/cm^2; 0.45 g/cm^3
B	1.6	1.4	50	20/10/20	$Al(OH)_3$; 0.5 mg/cm^2; 0.50 g/cm^3
C	1.6	1.4	70	15/14/15	$Al(OH)_3$; 0.5 mg/cm^2; 0.36 g/cm^3
D	1.9	1.8	30	20/10/20	$Al(OH)_3$; 0.5 mg/cm^2; 0.50 g/cm^3
E	1.9	1.8	50	15/15/15	$Al(OH)_3$; 0.5 mg/cm^2; 0.33 g/cm^3
F	1.9	1.8	70	20/13/20	$Al(OH)_3$; 0.5 mg/cm^2; 0.38 g/cm^3
G	1.9	1.8	30	20/10/20	nGO[a]; 0.1 mg/cm^2; 0.10 g/cm^3
H	1.9	1.8	30	20/10/20	$Al(OH)_3$; 1.0 mg/cm^2; 1.0 g/cm^3
I	1.9	1.8	30	20/10/20	$Zr(OH)_4$; 1.0 mg/cm^2; 1.0 g/cm^3
J	1.9	1.8	30	20/10/20	Al_2O_3; 1.0 mg/cm^2; 1.0 g/cm^3
K	1.9	1.8	30	20/10/20	no catalyst

[a]Nanographene oxide.

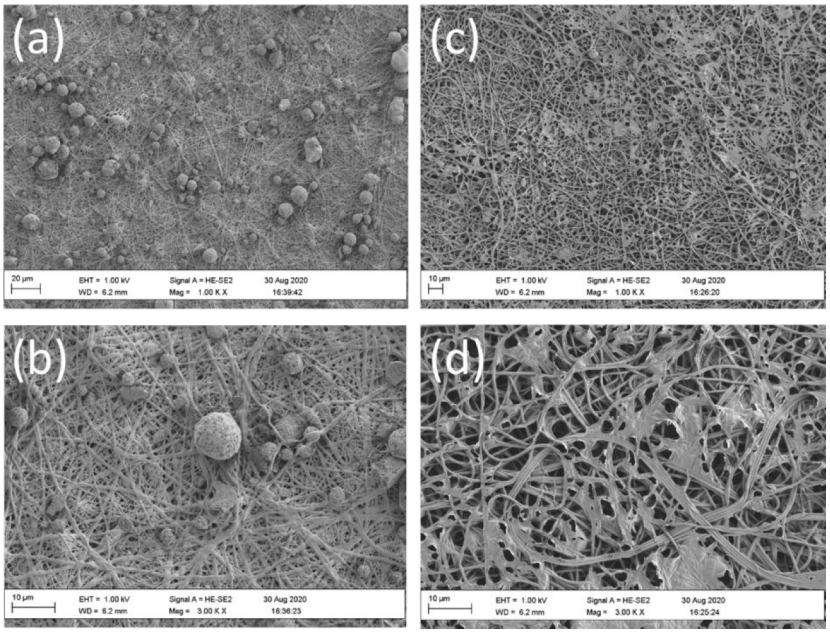

Figure 4. Top-down SEM images of electrospun bipolar junction mats with (a, b) $Al(OH)_3$ nanoparticles and (c, d) nGO particles. Significant aggregation of $Al(OH)_3$ and nGO is evident. Magnification: 1000× for (a) and (c) and 3000× for (b) and (d).

junction layer between 10 and 15 μm thick. For membranes A−F, the IEC and ratio of anion and cation-exchange ionomers in the 3D junction was varied. The catalyst type and areal loading were held constant ($Al(OH)_3$ particles at 0.5 mg/cm^2), but the volumetric loading differed due to changes in the dual fiber junction layer thickness. For membranes G−J, the IEC of SPEEK and QPPO and the thickness of each layer of the trilayer BPM were held constant, and the type and volumetric loading of catalyst in the 3D junction were varied. For comparison purposes, membrane K was a trilayer BPM with no catalyst in the 3D junction.

Figure 4a−d shows a dual fiber junction mat with a single layer of sprayed catalyst, $Al(OH)_3$ in Figure 4a,b and nGO in Figure 4c,d. The QPPO and SPEEK fibers are indistinguishable, as was also the case with high magnification SEMs. For the fiber mats shown in Figure 4, the average diameter was

https://doi.org/10.1021/acsami.2c07680
ACS Appl. Mater. Interfaces 2022, 14, 36092−36104

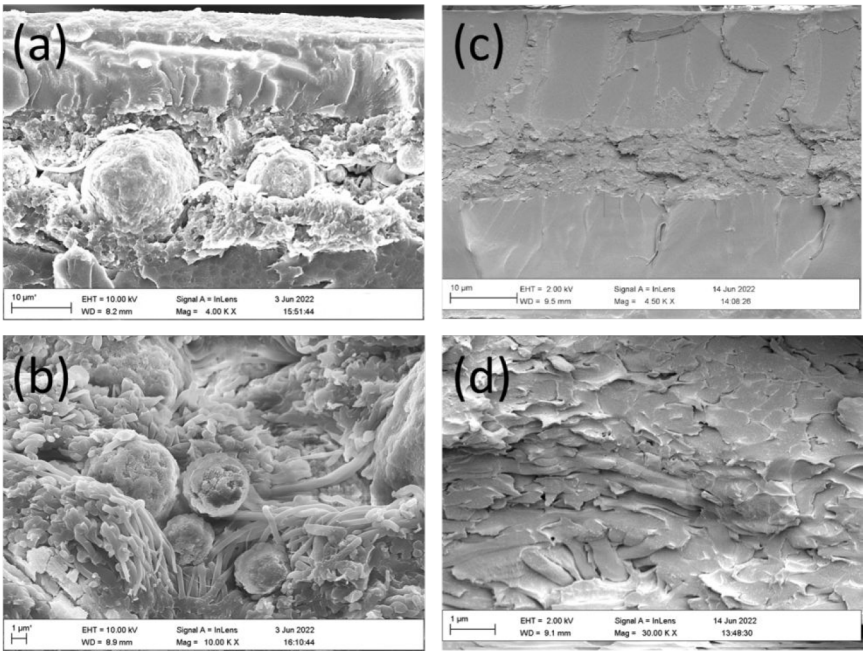

Figure 5. Cross-section SEM images of electrospun BPMs with (a, b) $Al(OH)_3$ nanoparticles and (c,d) nGO nanoparticles. Magnified sections of the respective junctions are shown in (b) and (d). Magnification: 4000× for (a), 10,000× for (b), 4500× for (c), and 30,000× for (d).

estimated to be 550 ± 50 nm. This fiber diameter is representative for all of the membranes listed in Table 3. There was no attempt in the present study to investigate the effect of fiber diameter on membrane performance. There is significant aggregation of $Al(OH)_3$ and nGO nanoparticles, with smaller domains of graphene oxide that are spread parallel to the junction surfaces and larger, spherical aggregates of $Al(OH)_3$ reaching nearly 10 μm in size.

In Figure 5, SEM cross-section images of BPMs with $Al(OH)_3$ and nGO catalyzed junctions are shown. For both BPMs, the junction layer appears to be well adhered to the dense outer films. High-magnification analysis of the junction regions (Figure 5b,d with $Al(OH)_3$ and nGO, respectively) confirms the earlier observation regarding $Al(OH)_3$ nanoparticle aggregation and their high volume fraction in the junction. Due to their high aspect ratio, single-nm thickness, and alignment parallel to the membrane surface, the nGO particles and their aggregates could not be identified in the cross-section image shown in Figure 5d.

Photographs of the raw dual fiber junction mat and the final trilayer membrane are shown in Figure 6a,b for membrane G in Table 3 (1.9 IEC SPEEK/1.8 IEC QPPO BPM with 0.1 mg/cm^2 nGO in the junction). As can be seen, the fully processed membrane, while transparent, is somewhat discolored (dark brown) due to the presence of nGO particles.

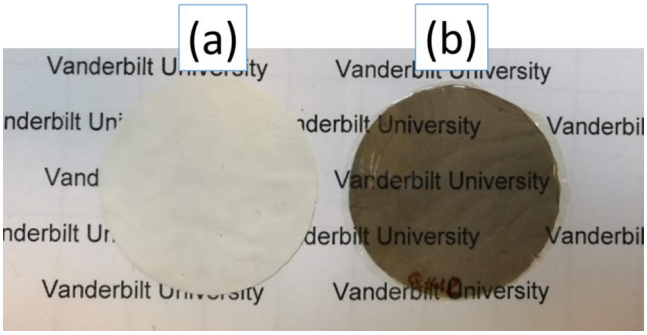

Figure 6. Photographs of: (a) Electrospun dual fiber junction layer with nGO-catalyst and (b) the final dense trilayer BPM.

3.2. Effect of Bipolar Junction Composition on BPM Performance. Galvanostatic current density vs voltage water splitting data for BPMs A–F, when immersed in 0.5 M Na_2SO_4, are shown in Figure 7a,b, along with a commercial Fumasep BPM from Fumatech and a BPM with a 3D junction made by sequential electrospinning of all three membrane layers.[18] As can be seen, all of the 3D junction BPMs from the present study were able to achieve a water splitting current density of 1000 mA/cm^2 at a reasonably low transmembrane voltage drop that was similar to that from ref 18. It can be concluded that attaching dense precast outside layers of AEP and CEP to a preformed dual fiber junction is a viable alternative membrane fabrication scheme to electrospinning the entire BPM. The lowest membrane voltage drop at 1000 mA/cm^2 (0.76 V) was achieved when the highest QPPO IEC (1.8 mmol/g) ionomer was used in both the junction and outer dense AEP layer. Also, there was no correlation between the volumetric concentration of $Al(OH)_3$ catalyst and the transmembrane voltage drop. The results in Figure 7 distinguish the operational high current density regime of 3D nanofiber junction BPMs from commercial membranes, like Fumasep, where the voltage drop increased significantly with a modest increase in current density. Such a large transmembrane voltage drop is unwanted and translates into high-energy consumption for water splitting.

The 3D junction BPMs were further characterized by examining more closely the onset potential for water splitting and the slope of the i–V curve during water splitting. Water dissociation occurs at the bipolar junction where CEP and AEP ionomers are in contact with one another and with a water splitting catalyst. When a BPM is operated in reverse bias mode at a low voltage, there is no ion transport (i.e., no current) because cations in solution cannot pass through the

https://doi.org/10.1021/acsami.2c07680
ACS Appl. Mater. Interfaces 2022, 14, 36092–36104

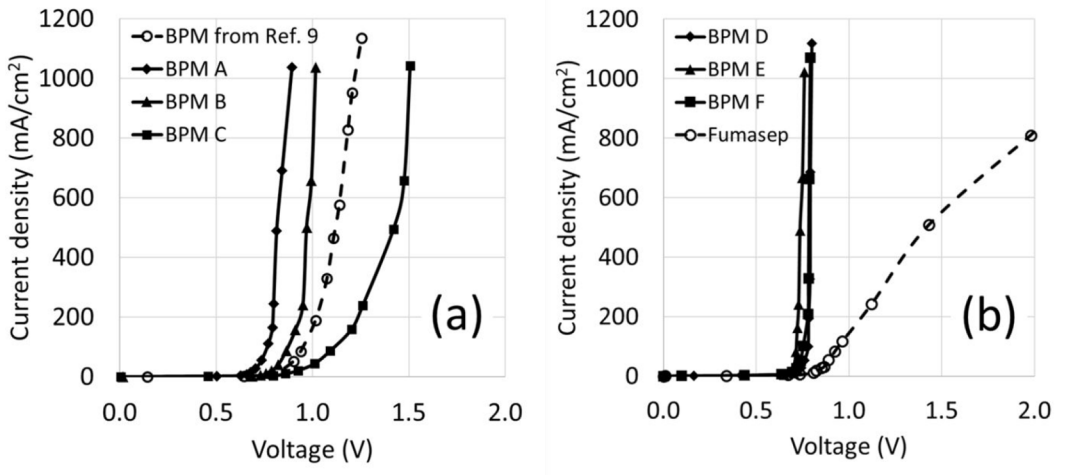

Figure 7. Current−voltage curves for BPMs with $Al(OH)_3$ at a loading of 0.5 mg/cm^2, utilizing (a) SPEEK (IEC = 1.6 mmol/g) and QPPO (IEC = 1.4 mmol/g) and (b) SPEEK (IEC = 1.9 mmol/g) and QPPO (IEC = 1.8 mmol/g). A Fumasep BPM is included for comparison.

AEP layer and anions cannot pass through the CEP layer, except for the possibility of small leakage currents due to defect pores or imperfect permselectivity of the ion-exchange layers. When the voltage is increased sufficiently, current flows because the initial equilibrium of water dissociation/association in the junction is shifted toward production of protons and hydroxide ions, which become the primary current carriers. During current flow, the potential difference (voltage) across a BPM is related to three major factors: (i) the pH difference at the junction, (ii) the water splitting activation overpotential, and (iii) the IR drop due to membrane resistance. The first contribution can be calculated based on the Nernst equation,[27] which for a pH difference of 13 (a pH of 14 for the alkaline side and a pH of 1 for the acid side) gives 0.828 V. The second contribution depends on the type of water splitting catalyst, where the activation overpotential is expected to be high for an uncatalyzed junction. The sum of these two contributions can be considered the open circuit potential (E_{OCV}), which was determined from an $i-V$ polarization plot as the intersection of two straight lines that are tangents to the low and high current density regimes (see Figure 8). The ion transport resistance in a BPM during water splitting, R_{WS}, was taken as the tangent to the $i-V$ curve at a high current density (>100 mA/cm^2). As can be seen by the results in Table 4, the values of E_{OCV} are low for 3D junction BPMs, indicating efficient generation of H^+ and OH^- at the junction. A high value of the water splitting potential, as per membrane C in Table 4, indicates a slow water splitting reaction (high activation overpotential). The values of R_{WS} in Table 4 for the catalyzed 3D junction BPMs are comparable to those reported by McDonald and Freund[6] for a 2D junction BPM composed of laminated Nafion and Neosepta AHA membranes with graphene oxide catalyst. The resistance of the Fumasep membrane was 3× greater than that of the best 3D junction BPM due to the overall greater thickness of this commercial film (~200 μm vs ~50 μm for a 3D junction BPM). The high value of R_{WS} for membrane C in Table 4 was the result of using low IEC AEP and CEP ionomers. Also, as expected, the lowest values of both E_{OCV} and R_{WS} were obtained with membranes D and E in Table 4, which were made with high IEC AEP and CEP polymers.

3.3. Effect of Catalyst Type on BPM Performance. Numerous studies on BPMs have reported on the importance

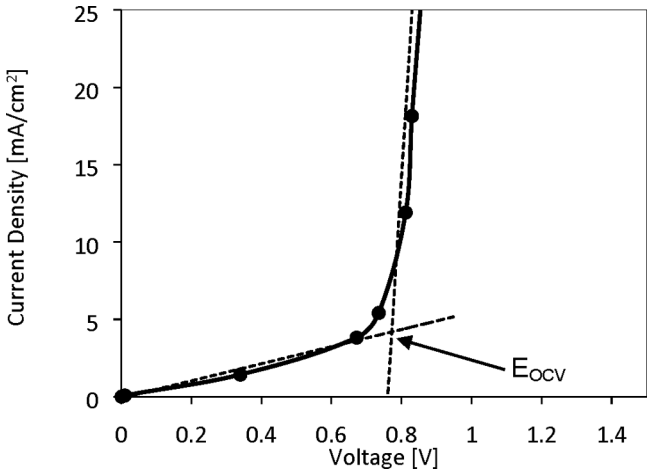

Figure 8. Estimation of the water splitting onset voltage (open circuit potential in a water splitting experiment, denoted as E_{OCV}) as the intersection of the two dashed tangent lines at the low current and high current sections of an $i-V$ curve.

Table 4. BPM Water Splitting Parameters of Merit (E_{OCV} and R_{WS})

membrane	E_{OCV} (V)	R_{WS} (Ω·cm^2)
A	0.68	0.203
B	0.78	0.458
C	0.91	0.721
D	0.75	0.153
E	0.71	0.097
F	0.72	0.245
Fumasep BPM	0.83	0.68

of catalyst particles in the water splitting junction. Various mechanisms were proposed wherein functional groups on the catalyst surface accelerated water dissociation.[28,29] In the present study, four different nanoparticle catalysts were evaluated in 3D junction BPMs: $Al(OH)_3$, nanographene oxide(nGO), $Zr(OH)_4$, and Al_2O_3. The same ionomers (1.9 IEC SPEEK and 1.8 IEC QPPO) were used for all membranes where the SPEEK/QPPO weight ratio in the junction was fixed at 30/70. Each catalyst was deposited in the dual fiber junction layer in the same way (by airbrush spraying during

https://doi.org/10.1021/acsami.2c07680
ACS Appl. Mater. Interfaces 2022, 14, 36092−36104

dual fiber electrospinning) and at the same areal loading (1.0 mg/cm^2), except nGO which was at a loading of 0.1 mg/cm^2. Current−voltage water splitting curves for these membranes in 0.5 M Na_2SO_4 are shown in Figure 9, along with a reference plot for a 3D junction BPM with no catalyst. Values of E_{OCV} and R_{WS} from the polarization curves in Figure 9 are listed in Table 5.

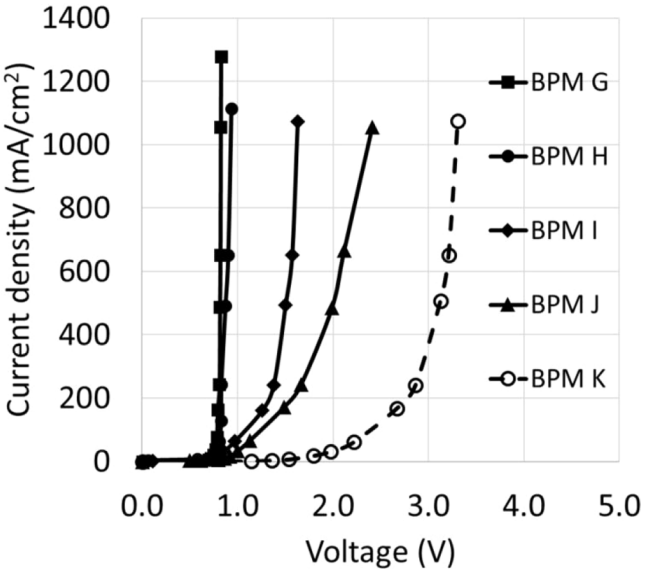

Figure 9. Current−voltage curves of BPMs containing different catalysts in the junction layer. (G) 0.1 g/cm^3 nGO (■); (H) 1.0 g/cm^3 $Al(OH)_3$ (●); (I) 1.0 g/cm^3 $Zr(OH)_4$ (◆); (J) 1.0 g/cm^3 Al_2O_3 (▲); and (K) no catalyst (○).

Table 5. Water Splitting Onset Potential (E_{OCV}) and Membrane Resistance to Ion Transport for 3D junction BPMs with Different Catalysts[a]

membrane	E_{OCV} (V)	R_{WS} (Ω·cm^2)
G	0.75	0.16
H	0.80	0.30
I	0.76	0.34
J	0.90	1.38
K (no catalyst)	1.82	1.21

[a]Membranes G−K are identified in the caption for Figure 9.

It is clear from Figure 9 that a catalyst is needed at the bipolar junction, but some particles work better than others. Even when the water splitting current is distributed over a very large AEP/CEP interpenetrating fiber network area, there is a large activation energy (voltage penalty) for generating acid and base in the absence of catalyst. Graphene oxide, which contains hydroxy and carboxy functional groups, worked well in 3D junction BPMs, as did $Al(OH)_3$ with hydroxy functionalities, although $Al(OH)_3$ is somewhat water-soluble (a solubility of 0.1 mg/100 mL in water), which may be a problem during long-term membrane operation. Similar to $Al(OH)_3$, Al_2O_3 is also amphoteric, but is insoluble in water. Its use might potentially improve the long-term stability of the membrane, as compared to $Al(OH)_3$, but this catalyst did not work well, with a measured voltage drop of >2.0 V at 1000 mA/cm^2, which was more than twice the voltage requirement of an nGO-catalyzed membrane. The relatively high values of both E_{OCV} and R_{WS} for Al_2O_3 (from Table 5) indicate moderate catalytic activity for water splitting and interference with the ion transport. The use of $Zr(OH)_4$ particles led to BPMs with low/desirable values of E_{OCV} and R_{WS} (membrane I), but there was a higher than expected activation energy for current densities in 10−170 mA/cm^2 range, resulting in a high transmembrane voltage drop (1.8 V) at 1000 mA/cm^2. Overall, these results are consistent with the water splitting mechanism suggested by Simons and others,[3,29,30] involving proton transfer between an acid and its conjugate base on ionizable groups within an ion exchange membrane. The presence of edge carboxylate groups in graphene oxide likely led to its excellent performance as a water splitting catalyst.[31] From the results in Figures 7 and 9 for membranes D−J (i.e., those membranes with 1.9 IEC SPEEK and 1.8 IEC QPPO), there was no correlation between the volumetric concentration of catalyst in the junction and the transmembrane voltage drop at high current densities (>500 mA/cm^2). The two best catalysts, nGO and $Al(OH)_3$, differed in surface area-to-volume ratio (nGO with the larger ratio) and in their morphology in the junction, with small domains of graphene oxide and larger aggregates of $Al(OH)_3$ (see Figure 4). This might be the reason for a higher specific activity of nGO, as it was necessary to use about 10 times more $Al(OH)_3$ as nGO to achieve the same water splitting performance. Overall, graphene oxide appears to be the best water splitting catalyst, with excellent activity, a low volumetric concentration in the junction, and no issue at the present time regarding long-term water solubility.

3.4. Co-Ion Leakage in 3D Junction BPMs. In order to determine the effect of salt type and concentration on co-ion leakage during water splitting, limiting current H-cell experiments[24] were performed with aqueous 0.5 and 1.0 M Na_2SO_4 solutions and with 1.0 and 2.0 M $NaNO_3$ solutions ($NaNO_3$ was used for higher salt concentration since it is more water-soluble than Na_2SO_4). The resultant $i-V$ curves are shown in Figure 10a−d. Currents observed below the onset voltage for water splitting are due to co-ion crossover. While the crossover currents for both salts are very low, the co-ion leakage is smaller in Na_2SO_4 solutions, due to better rejection of divalent sulfate anions, as compared to monovalent nitrate anions (Figure 10b,d, with expanded current density axes, clearly shows the difference in crossover between Na_2SO_4 and $NaNO_3$). Based on these plots, co-ion crossover is <0.25 mA/cm^2 for Na_2SO_4 and <0.5 mA/cm^2 $NaNO_3$. These current densities are quite small, indicating no pinhole defects in the 3D junction BPMs and adequate co-ion rejection by the high IEC CEP and AEP dense outer layers.

An additional experiment to measure co-ion leakage and pH change was performed in a four-compartment cell that was filled with 0.5 M Na_2SO_4 solution (Figure 11). This experiment was carried out with a 75 μm-thick 3D junction BPM (a 17 μm dry thickness junction with 1.6 IEC SPEEK and 1.5 IEC QPPO nanofibers with 0.06 g/cm^3 n-GO, a 31 μm outer layer of 1.6 IEC SPEEK, and a 27 μm outer layer of 1.5 IEC QPPO). The measured initial and final values of Na^+ and SO_4^{2-} concentration, and pH in the acidic and the alkaline compartments (the two compartments that were separated by the BPM) are listed in Table 6. As can be seen, the solution pH in the acidic compartment decreased from 5.8 to 1.1, while that in the alkaline compartment increased from 5.8 to 13.3. These pH changes indicate effective water splitting by the BPM and are consistent with the anticipated H^+ and OH^- changes based on the applied current (1.4 A), time (10 min), and solution volume (15 mL for each compartment). The Na^+ concen-

https://doi.org/10.1021/acsami.2c07680
ACS Appl. Mater. Interfaces 2022, 14, 36092−36104

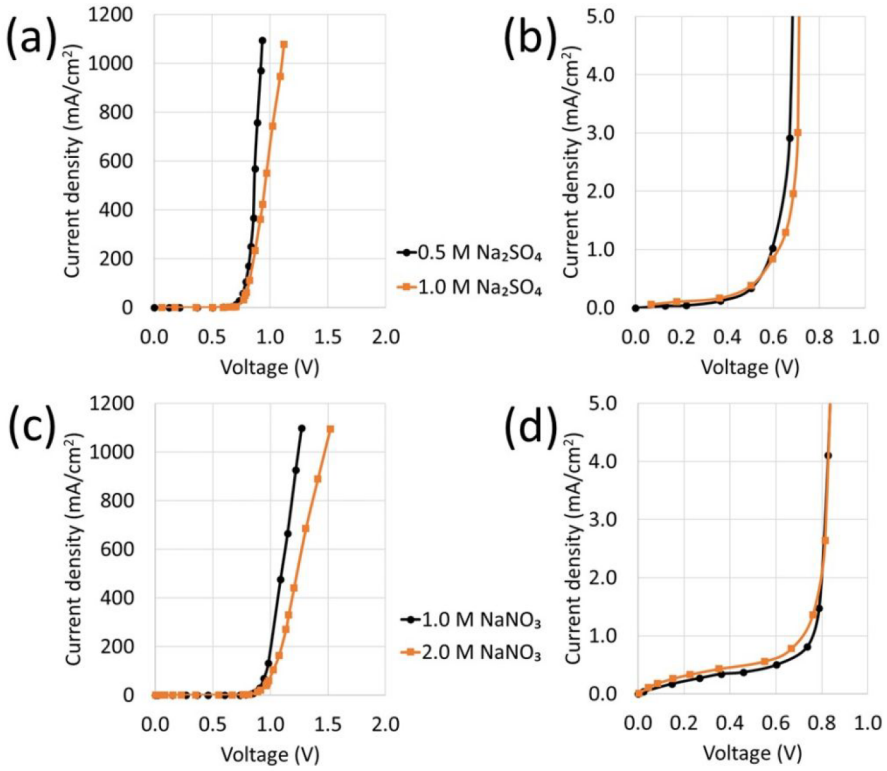

Figure 10. Water splitting $i-V$ polarization curves for different external salt solutions. The 3D junction BPM was composed of 1.8 IEC SPEEK/n-GO/1.7 IEC QPPO (58 μm total dry thickness). (a, c) Full polarization curves up to 1100 mA/cm^2. (b, d) Expanded views of the low current density portion of the polarization curves.

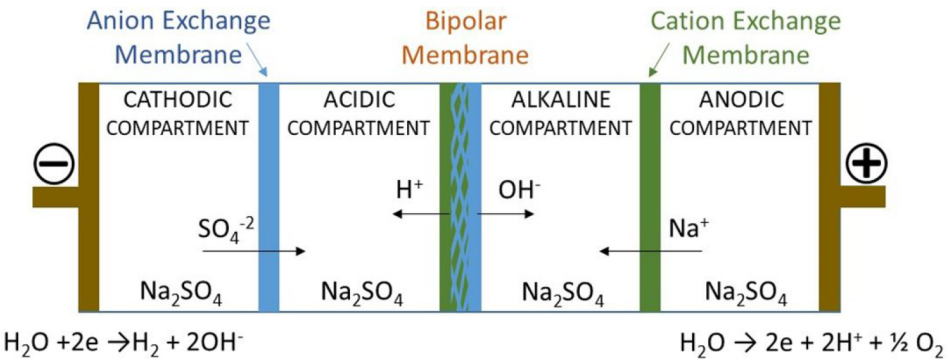

Figure 11. Schematic diagram of the electrodialysis cell for the determination of co-ion leakage and pH changes through a 3D junction BPM during constant current water splitting.

Table 6. Initial and Final Values of pH and Sodium/Sulfate Ion Concentrations in the Acidic and the Alkaline Compartments Separated by a 3D Junction BPM in a Water Splitting Experiment

	acidic compartment (H_2SO_4 generation)		alkaline compartment (NaOH generation)	
	pH	Na^+ concentration (mol/L)	pH	SO_4^{2-} concentration (mol/L)
initial	5.8	0.97	5.8	0.50
after water splitting at 0.2 A/cm^2 for 10 min	1.1	0.96	13.3	0.47

tration in the acidic compartment and the SO_4^{-2} concentration in the alkaline compartment remained constant (within the precision of the ICP analytic method), indicating: (i) there was no co-ion crossover through the BPM, (ii) the H^+ and OH^- concentrations near the anode and cathode were small as compared to 0.5 M Na_2SO_4, with no proton or hydroxide leakage into the acid and alkaline compartments, and (iii) the anion exchange and cation exchange membranes in the cell were perfectly permselective. Both (ii) and (iii) are reasonable, given the low charge passed in the short-time experiment and the high IEC of the anion and cation exchange membranes. Based on these results and those in Figure 10, it can be concluded that the 3D junction BPMs adequately block unwanted co-ion leakage during constant current water splitting operation, with a current efficiency for water splitting >99% for current densities between 0.2 A/cm^2 and 1.0 A/cm^2.

3.5. Comparison with Literature Data. The water splitting current–voltage performance of a number of representative BPMs in the literature is summarized in Table

https://doi.org/10.1021/acsami.2c07680
ACS Appl. Mater. Interfaces 2022, 14, 36092−36104

Table 7. Summary of water splitting performance of BPMs in the literature

AEP	CEP	catalyst	water splitting performance	ref
QPPO	SPEEK	graphene oxide	0.79 V @ 160 mA/cm^2, 0.824 V@ 1300 mA/cm^2	this paper
Neosepta AHA	Nafion	graphene oxide	1.05 V @ 100 mA/cm^2	6
quaternized polysulfone	sulfonated polysulfone	phosphorylated graphene oxide/quaternized graphene oxide	6 V @ 60 mA/cm^2	7
modified chitosan	sodium alginate	copper phthalocyanine tetrasulfonic acid	5.6 V @ 120 mA/cm^2	32
quaternized chitosan	*N*-methylene phosphonic chitosan	polyethylene glycol	5 V @ 55 mA/cm^2	33
aminated polystyrene	sulfonated poly(ether sulfone)	silicon alkoxide	11 V @ 120 mA/cm^2	34
quaternized PPO	sulfonated PPO	Fe-MIL-101-NH_2	4.5 V @ 120 mA/cm^2	35
quaternized polysulfone	sulfonated polysulfone	lysozyme	5 V @ 65 mA/cm^2	36
polyepichlorohydrin/ polyvinylidene fluoride	sulfonated poly(ether sulfone)	MoS_2	4.2 V @ 58 mA/cm^2	37
commercial membrane	commercial membrane	Fe complex ($K_4[Fe(CN)_6]$ + $FeCl_3$)	12 V @ 108.9 mA/cm^2	38
QPPO	carboxylated polyacrylonitrile	Fe (III) @ PEI (polyethylenimine)	1.88 V @ 320 mA/cm^2	39

7 and compared with the 3D junction BPM data in this paper. Most publications describe BPMs that exhibit a high transmembrane voltage drop at a low current density and no membrane was tested above 320 mA/cm^2. The low operating voltage and high operating currrent density of the 3D junction membranes in the present study (<1.0 V at 1000 mA/cm^2) is in stark contrast to the literature data. Such a low voltage drop is not unreasonable, given the conductivity of the SPEEK and QPPO ionomers, the amount of each ionomer, and the overall thickness of the membrane. A simple membrane resistance analysis was used to verify this point, where the overall areal resistance of a 3D junction BPM (R, with units of Ω·cm^2) was calculated as the sum of the resistances of the AEP, CEP, and junction layers:

$$R_{BPM} = \frac{\Delta x_{AEP}}{\kappa_{AEP}} + R_J + \frac{\Delta x_{CEP}}{\kappa_{CEP}} \quad (6)$$

The areal resistance of the electrospun, uncatalyzed 3D dual-fiber junction (R_J) was modeled as a parallel array of AEP and CEP fibers (a tortuosity of 1.0 for H^+ and OH- pathways):

$$\frac{1}{R_{J_o}} = \frac{\theta}{R_{CEF}} + \frac{(1-\theta)}{R_{AEF}} \quad (7)$$

where R_{CEF} and R_{AEF} are the areal resistances of the cation exchange and anion exchange polymer fibers in the junction, respectively, and θ is the volume fraction of cation exchange fibers in the junction. R_{J_o} in eq 7 was further modified to take into account ion-impermeable catalyst particles in the junction that will increase the junction resistance by: (1) reducing the ion conducting cross-sectional area of the junction and (2) creating a more tortuous pathway for ion migration. Based on the Maxwell equation,[40] the resistances in the presence and absence of particles (R_J and R_{J_o}) in a polymer/particle composite material (junction layer) are related to one another by

$$\frac{R_J}{R_{J_o}} = 1 + \frac{\alpha^2\varphi^2}{1-\varphi} \quad (8)$$

where φ is volume fraction of particles and α is the particle aspect ratio.

In the present analysis, the calculated values of R_{BPM} from eqs 6−8 and the conductivity and layer thickness data in Tables 2 and 3 were matched to the R_{WS} data in Table 4, using the aspect ratio for $Al(OH)_3$ particles as an adjustable parameter. For eq 7, the weight fractions of AEP and CEP fibers in the junction from Table 3 were converted to volume fractions, assuming equal polymer densities for SPEEK and QPPO. For eq 8, the areal loading of $Al(OH)_3$ particles in the junction (0.5 mg/cm^2) was converted to particle volume fraction using a particle density of 2.5 g/cm^3 and the junction thickness data in Table 3.

As shown in Table 8, the calculated areal resistances of BPMs with an uncatalyzed junction are far below the experimentally measured resistances. When the resistance of $Al(OH)_3$ particles in the junction layer was added to the analysis, using the particle aspect ratio as an adjustable parameter, a near-exact match of the calculated and experimental membrane areal resistances was achieved. The best-fit (optimized) values of α are listed in Table 8. The $Al(OH)_3$ catalyst particles are known to be spherical in shape, with a diameter of ∼10 nm, so the high aspect ratios in Table 8 indicate clustering of these particles in the junction, which was qualitatively observed in the SEMs of a dual fiber junction (see Figures 4 and 5). Smaller aspect ratios would have been obtained if the R_{AEF} and R_{ECF} in eq 7 accounted for the tortuosity of ion transport pathways in the junction layer. It should also be noted that the conductivities used in eq 6 were measured for membranes immersed in water and not in a 0.5

Table 8. Calculated Areal Resistance of BPMs in the Absence of $Al(OH)_3$ Particles and Experimentally Measured Resistances, for Membranes A−F from Table 3

BPMs	calculated resistance of BPMs with uncatalyzed junction (Ω·cm^2)	experimentally measured resistance[a] (Ω·cm^2)[a]	particle aspect ratio (α)^2
A	0.192	0.203	2.57
B	0.183	0.468	13.14
C	0.154	0.721	24.63
D	0.099	0.153	7.28
E	0.086	0.097	4.51
F	0.100	0.245	16.04

[a]From Table 4.

https://doi.org/10.1021/acsami.2c07680
ACS Appl. Mater. Interfaces 2022, 14, 36092−36104

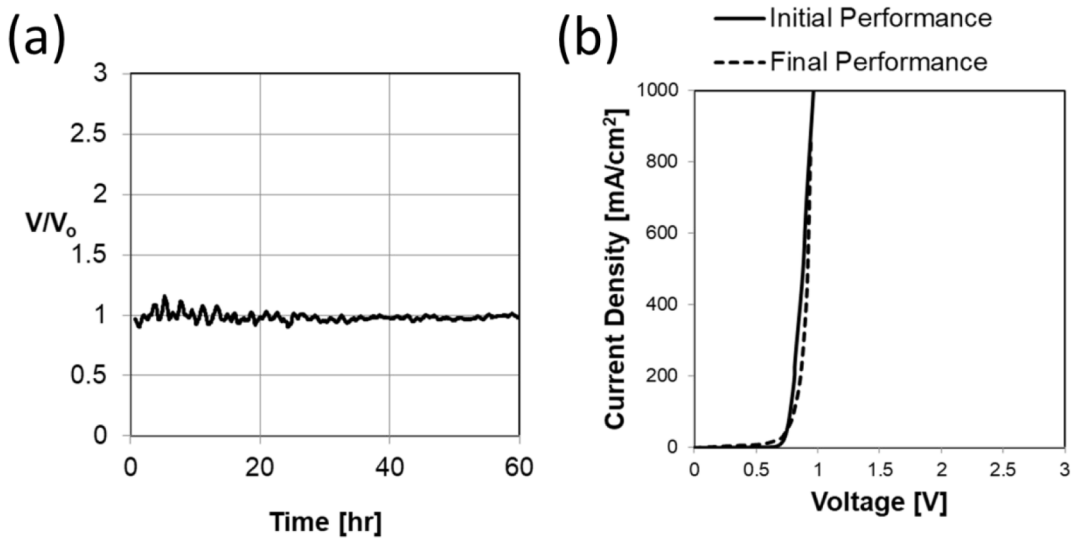

Figure 12. Results of a long-time constant current water splitting experiment at 800 mA/cm^2 and 30 °C. (a) Normalized membranes voltage drop vs time and (b) $i-V$ polarization curves at 0 h and at 60 h. The BPM was composed of 1.9 IEC SPEEK and 1.8 IEC QPPO with nGO catalyst in the junction layer (60 μm total dry membrane thickness).

M Na_2SO_4 solution, but the difference in κ should be small due to the very high IEC of both the SPEEK and QPPO relative to the electrolyte concentration, with good co-ion/salt exclusion (if co-ion sorption were significant, the theoretical model calculations for resistance would be greater than those measured experimentally, which is not the case).

3.6. BPM Durability Testing. BPM durability (the stability of the measured transmembrane voltage during BPM operation over an extended time) was determined by a galvanostatic constant current water splitting experiment at 30 °C. A 1.9 IEC SPEEK/1.8 IEC QPPO BPM with a 0.1 mg/cm^2 nGO catalyzed junction was selected for this test (same membrane as shown in Figure 6). The results of this experiment are shown in Figure 12a, where the normalized transmembrane voltage drop (V/V_0, where V_0 is the initial voltage drop) is plotted versus time. The data were smoothed using Matlab's moving average function in order to minimize fluctuations in the voltage measurements caused by gas bubbles evolving from the electrodes. As can be seen, the 3D junction BPM exhibited stable performance during this long-time test (an increase in voltage of <5%, which is within the experimental accuracy of the measurement equipment). Upon removal of the electrolyte-swollen membrane from the H-cell, there was no apparent physical damage and no evidence of delamination. Additionally, $i-V$ water splitting curves were recorded at the beginning and the end of the test. As shown in Figure 12b, the plots overlap, with no change in either E_{OCV} or R_{WS}.

4. CONCLUSIONS

Bipolar membranes with a nanofiber-based 3D junction were fabricated and evaluated. A new and simpler method of preparing the membranes (compared to that reported earlier)[18] was developed, where electrospinning was only used to make the dual fiber bipolar junction layer. Precast dense outer films of anion and cation-exchange polymers were then hot-pressed onto the junction layer to complete the fabrication process. Membranes were prepared with QPPO as the anion exchange polymer and SPEEK as the cation exchange polymer, with various junction layer catalysts.

The 3D junction membranes were able to split water at very high rates (up to 1000 mA/cm^2) and at a low transmembrane voltage drop (approximately 0.8 V). The nGO at a very low loading (0.1 g/cm^3) worked best as the water splitting catalyst in the junction layer. The 3D junction membranes exhibited excellent stability during a 60 h water splitting experiment at a constant current density of 800 mA/cm^2, with essentially no change in transmembrane voltage drop over time and no visual indication of membrane degradation/delamination. Co-ion leakage was low with crossover current densities of no more than 0.5 mA/cm^2 for external salt solutions up to 2.0 M. The low operating voltage was associated with efficient water splitting in the junction layer (a low onset potential for water splitting) due to a high interfacial area catalyzed junction and the use of thin membranes composed of high IEC ionomers. The excellent high current density durability of the BPMs was due to the interpenetrating and interlocking polymer fiber morphology of the 3D junction and good adherence of the dense AEP and CEP outer films to the junction layer. Based on the observed performance metrics, 3D junction BPMs show great promise for use in electrochemical separations, electrolysis cells, and energy conversion/storage applications.

AUTHOR INFORMATION

Corresponding Author

Peter N. Pintauro − *Department of Chemical and Biomolecular Engineering, Vanderbilt University, Nashville, Tennessee 37235, United States;* orcid.org/0000-0001-5115-7276; Email: pn.pintauro@vanderbilt.edu

Authors

Devon Powers − *Department of Chemical and Biomolecular Engineering, Vanderbilt University, Nashville, Tennessee 37235, United States*

Abhishek N. Mondal − *Department of Chemical and Biomolecular Engineering, Vanderbilt University, Nashville, Tennessee 37235, United States*

Zezhou Yang − *Department of Chemical and Biomolecular Engineering, Vanderbilt University, Nashville, Tennessee 37235, United States*

https://doi.org/10.1021/acsami.2c07680
ACS Appl. Mater. Interfaces 2022, 14, 36092−36104

Ryszard Wycisk − *Department of Chemical and Biomolecular Engineering, Vanderbilt University, Nashville, Tennessee 37235, United States*
Eric Kreidler − *Honda R&D Americas, LLC, Raymond, Ohio 43067, United States*

Complete contact information is available at: https://pubs.acs.org/10.1021/acsami.2c07680

Notes

The authors declare no competing financial interest.

■ ACKNOWLEDGMENTS

This study was funded by grants from the ARPA-E, grant no. DE-AR0001035, and the Honda Research Institute.

■ REFERENCES

(1) McDonald, M. B.; Bruce, J. P.; McEleney, K.; Freund, M. S. Reduced Graphene Oxide Bipolar Membranes for Integrated Solar Water Splitting in Optimal pH. *ChemSusChem* **2015**, *8*, 2645−2654.
(2) Mani, K. N. Electrodialysis Water Splitting Technology. *J. Membr. Sci.* **1991**, *58*, 117−138.
(3) Xue, Y.; Wang, N.; Huang, C.; Cheng, Y.; Xu, T. Catalytic Water Dissociation at the Intermediate Layer of a Bipolar Membrane: The Role of Carboxylated Boltorn® H30. *J. Membr. Sci.* **2009**, *344*, 129−135.
(4) Tanioka, A.; Shimizu, K.; Hosono, T.; Eto, R.; Osaki, T. Effect of Interfacial State in Bipolar Membrane on Rectification and Water Splitting. *Colloids Surf., A* **1999**, *159*, 395−404.
(5) Balster, J.; Srinkantharajah, S.; Sumbharaju, R.; Pünt, I.; Lammertink, R. G. H.; Stamatialis, D. F.; Wessling, M. Tailoring the Interface Layer of the Bipolar Membrane. *J. Membr. Sci.* **2010**, *365*, 389−398.
(6) Mcdonald, M. B.; Freund, M. S. Graphene Oxide as a Water Dissociation Catalyst in the Bipolar Membrane Interfacial Layer. *ACS Appl. Mater. Interfaces* **2014**, *6*, 13790−13797.
(7) Manohar, M.; Das, A. K.; Shahi, V. K. Efficient Bipolar Membrane with Functionalized Graphene Oxide Interfacial Layer for Water Splitting and Converting Salt into Acid/Base by Electrodialysis. *Ind. Eng. Chem. Res.* **2018**, *57*, 1129−1136.
(8) Manohar, M.; Shahi, V. K. Graphene Oxide-Polyaniline as a Water Dissociation Catalyst in the Interfacial Layer of Bipolar Membrane for Energy-Saving Production of Carboxylic Acids from Carboxylates by Electrodialysis. *ACS Sustain. Chem. Eng.* **2018**, *6*, 3463−3471.
(9) Giesbrecht, P. K.; Freund, M. S. Recent Advances in Bipolar Membrane Design and Applications. *Chem. Mater.* **2020**, *32*, 8060−8090.
(10) Blommaert, M. A.; Aili, D.; Tufa, R. A.; Li, Q.; Smith, W. A.; Vermaas, D. A. Insights and Challenges for Applying Bipolar Membranes in Advanced Electrochemical Energy Systems. *ACS Energy Letters* **2021**, *6*, 2539−2548.
(11) Pärnamäe, R.; Mareev, S.; Nikonenko, V.; Melnikov, S.; Sheldeshov, N.; Zabolotskii, V.; Hamelers, H. V. M.; Tedesco, M. Bipolar Membranes: A Review on Principles, Latest Developments, and Applications. *J. Membr. Sci.* **2021**, *617*, 118538.
(12) Daud, S. N. S. S.; Jaafar, J.; Norddin, M. N. A. N.; Sudirman, R.; Onuomo, O. J.; Ismail, A. F.; Othman, M. H. D.; Rahman, M. A.; Alias, N. H.; Junoh, H. A Review on Process Design and Bilayer Electrolyte Materials of Bipolar Membrane Fuel Cell. *Int. J. Energy Res.* **2022**, *46*, 11620−11639.
(13) Kole, S.; Venugopalan, G.; Bhattacharya, D.; Zhang, L.; Cheng, J.; Pivovar, B.; Arges, C. G. Bipolar Membrane Polarization Behavior with Systematically Varied Interfacial Areas in the Junction Region. *J. Mater. Chem. A* **2021**, *9*, 2223−2238.
(14) Oener, S. Z.; Foster, M. J.; Boettcher, S. W. Accelerating Water Dissociation in Bipolar Membranes and for Electrocatalysis. *Science* **2020**, *369*, 1099−1103.
(15) Ahehzad, M. A.; Yasmin, A.; Ge, X.; Ge, Z.; Zhang, K.; Liang, X.; Zhang, J.; Li, G.; Xiao, X.; Jiang, B.; Wu, L.; Xu, T. Shielded Goethite Catalyst that Enables Fast Water Dissociation in Bipolar Membranes. *Nat. Commun.* **2021**, *12*, 9.
(16) Wakamatsu, Y.; Matsumoto, H.; Minagawa, M.; Tanioka, A. Effect of Ion-Exchange Nanofiber Fabrics on Water Splitting in Bipolar Membrane. *J. Colloid Interface Sci.* **2006**, *300*, 442−445.
(17) Mayerhöfer, B.; McLaughlin, D.; Böhm, T.; Hegelheimer, M.; Seeberger, D.; Thiele, S. Bipolar Membrane Electrode Assemblies for Water Electrolysis. *ACS Appl. Energy Mater.* **2020**, *3*, 9635−9644.
(18) Shen, C.; Wycisk, R.; Pintauro, P. N. High Performance Electrospun Bipolar Membrane with a 3D Junction. *Energy Environ. Sci.* **2017**, *10*, 1435−1442.
(19) Robertson, G. P.; Mikhailenko, S. D.; Wang, K.; Xing, P.; Guiver, M. D.; Kaliaguine, S. Casting Solvent Interactions with Sulfonated Poly(Ether Ether Ketone) During Proton Exchange Membrane Fabrication. *J. Membr. Sci.* **2003**, *219*, 113−121.
(20) Swier, S.; Shaw, M. T.; Weiss, R. A. Morphology Control of Sulfonated Poly(Ether Ketone Ketone) Poly(Ether Imide) Blends and Their Use in Proton-Exchange Membranes. *J. Membr. Sci.* **2006**, *270*, 22−31.
(21) Xu, T.; Yang, W. Fundamental Studies on a Novel Series of Bipolar Membranes Prepared from Poly(2,6-Dimethyl-1,4-Phenylene Oxide) (PPO) I. Effect of Anion Exchange Layers on I-V Curves of Bipolar Membranes. *J. Membr. Sci.* **2004**, *238*, 123−129.
(22) Park, A. M.; Wycisk, R. J.; Ren, X.; Turley, F. E.; Pintauro, P. N. Crosslinked Poly(Phenylene Oxide)-Based Nanofiber Composite Membranes for Alkaline Fuel Cells. *J. Mater. Chem. A* **2016**, *4*, 132−141.
(23) Choi, J.; Wycisk, R.; Zhang, W.; Pintauro, P. N.; Lee, K. M.; Mather, P. T. High Conductivity Perfluorosulfonic Acid Nanofiber Composite Fuel-Cell Membranes. *ChemSusChem* **2010**, *3*, 1245−1248.
(24) Strathmann, H.; Krol, J. J.; Rapp, H.-J.; Eigenberger, G. Limiting Current Density and Water Dissociation in Bipolar Membranes. *J. Membr. Sci.* **1997**, *125*, 123−142.
(25) Huang, R. Y. M.; Shao, P.; Burns, C. M.; Feng, X. Sulfonation of Poly(Ether Ether Ketone) (PEEK): Kinetic Study and Characterization. *J. Appl. Polym. Sci.* **2001**, *82*, 2651−2660.
(26) Jiang, R.; Kunz, H. R.; Fenton, J. M. Investigation of Membrane Property and Fuel Cell Behavior with Sulfonated Poly(Ether Ether Ketone) Electrolyte: Temperature and Relative Humidity Effects. *J. Power Sources* **2005**, *150*, 120−128.
(27) Strathmann, H.; Rapp, H.-J.; Bauer, B.; Bell, C. M. Theoretical and Practical Aspects of Preparing Bipolar Membranes. *Desalination* **1993**, *90*, 303−323.
(28) Kang, M.; Choi, Y.; Moon, S. Effects of Inorganic Substances on Water Splitting in Ion-Exchange Membranes II. Optimal Contents of Inorganic Substances in Preparing Bipolar Membranes. *J. Colloid Interface Sci.* **2004**, *273*, 533−539.
(29) Simons, R. Water Splitting in Ion Exchange Membranes. *Electrochim. Acta* **1985**, *30*, 275−282.
(30) Simons, R. Strong Electric Field Effects on Proton Transfer Between Membrane-Bound Amines and Water. *Nature* **1979**, *280*, 824−826.
(31) Martínez, R. J.; Farrell, J. Water Splitting Activity of Oxygen-Containing Groups in Graphene Oxide Catalyst in Bipolar Membranes. *Computational and Theoretical Chemistry* **2019**, *1164*, 112556.
(32) Chen, R.; Chen, Z.; Zheng, X.; Chen, X.; Wu, S. Preparation and Characterization of mSA/mCS Bipolar Membranes Modified by CuTsPc and CuTAPc. *J. Membr. Sci.* **2010**, *355*, 1−6.
(33) Rajesh, A. M.; Kumar, M.; Shahi, V. K. Functionalized Biopolymer Based Bipolar Membrane with Poly Ethylene Glycol Interfacial Layer for Improved Water Splitting. *J. Membr. Sci.* **2011**, *372*, 249−257.
(34) Rajesh, A. M.; Chakrabarty, T.; Prakash, S.; Shahi, V. K. Effects of Metal Alkoxides on Electro-Assisted Water Dissociation Across Bipolar Membranes. *Electrochim. Acta* **2012**, *66*, 325−331.

(35) Wang, Q.; Wu, B.; Jiang, C.; Wang, Y.; Xu, T. Improving the Water Dissociation Efficiency in a Bipolar Membrane with Amino-Functionalized MIL-101. *J. Membr. Sci.* **2017**, *524*, 370−376.
(36) Manohar, M.; Shukla, G.; Pandey, R. P.; Shahi, V. K. Efficient Bipolar Membrane with Protein Interfacial Layer for Optimal Water Splitting. *Journal of Industrial and Engineering Chemistry* **2017**, *47*, 141−149.
(37) Li, J.; Morthensen, S. T.; Zhu, J.; Yuan, S.; Wang, J.; Volodine, A.; Lin, J.; Shen, J.; Van der Bruggen, B. Exfoliated MoS_2 Nanosheets Loaded on Bipolar Exchange Membranes Interfaces as Advanced Catalysts for Water Dissociation. *Sep. Purif. Technol.* **2018**, *194*, 416−424.
(38) Cheng, G.; Zhao, Y.; Li, W.; Zhang, J.; Wang, X.; Dong, C. Performance Enhancement of Bipolar Membranes Modified by Fe Complex Catalyst. *J. Membr. Sci.* **2019**, *589*, 117243.
(39) Ge, Z.; Shehzad, M. A.; Ge, L.; Zhu, Y.; Wang, H.; Li, G.; Zhang, J.; Ge, X.; Wu, L.; Xu, T. Beneficial Use of a Coordination Complex as the Junction Catalyst in a Bipolar Membrane. *ACS Appl. Energy Mater.* **2020**, *3*, 5765−5773.
(40) Cussler, E. L.; Hughes, S. E.; Ward, W. J.; Aris, R. Barrier Membranes. *J. Membr. Sci.* **1988**, *38*, 161−174.

https://doi.org/10.1021/acsami.2c07680
ACS Appl. Mater. Interfaces 2022, 14, 36092−36104